LANGMUIR

Article

pubs.acs.org/Langmuir

Imparting Icephobicity with Substrate Flexibility

Thomas Vasileiou, Thomas M. Schutzius,* and Dimos Poulikakos*

Laboratory of Thermodynamics in Emerging Technologies, Department of Mechanical and Process Engineering, ETH Zurich, Sonneggstrasse 3, CH-8092 Zurich, Switzerland

Supporting Information

ABSTRACT: Ice accumulation hinders the performance of, and poses safety threats for, infrastructure both on the ground and in the air. Previously, rationally designed superhydrophobic surfaces have demonstrated some potential as a passive means to mitigate ice accretion; however, further studies on material solutions that reduce impalement and the contact time for impacting supercooled droplets (high viscosity) and can also repel droplets that freeze during surface contact are urgently needed. Here we demonstrate the collaborative effect of substrate flexibility and surface micro/nanotexture on enhancing both icephobicity and the repellency of viscous droplets (typical of supercooled water). We first investigate the influence of increased viscosity (spanning from 0.9 to 1078 mPa·s using water−glycerol mixtures) on impalement resistance and the droplet−substrate contact time after impact. Then we examine the effect of droplet partial solidification on recoil and simulate more challenging icing conditions by impacting supercooled water droplets (down to −15 °C) onto flexible and rigid surfaces containing ice nucleation promoters (AgI). We demonstrate a passive mechanism for shedding partially solidified (recalescent) droplets—under conditions where partial solidification occurs much faster than the natural droplet oscillation—which does not rely on converting droplet surface energy into kinetic energy (classic recoil mechanism). Using an energy-based model (kinetic−elastic−capillary), we identify a previously unexplored mechanism whereby the substrate oscillation and velocity govern the rebound process, with low areal density and moderately stiff substrates acting to efficiently absorb the incoming droplet kinetic energy and rectify it back, allowing droplets to overcome adhesion and gravitational forces, and recoil. This mechanism applies for a range of droplet viscosities, spanning from low- to high-viscosity fluids and even ice slurries, which do not rebound from rigid superhydrophobic substrates. For a low-viscosity fluid, i.e., water, if the substrate oscillates faster than the droplet spreading and retraction, the action of the substrate is decoupled from the droplet oscillation, resulting in a reduction in the droplet−substrate contact time.

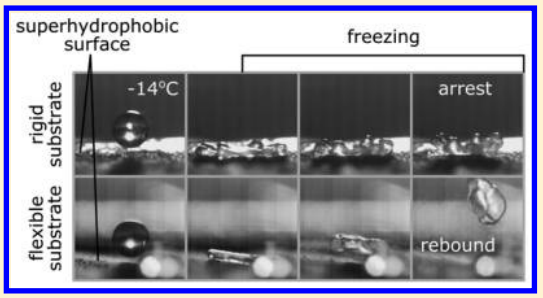

INTRODUCTION

Much of the modern infrastructure exposed to the open atmosphere is susceptible to surface icing, which can compromise aircraft airworthiness,[1,2] hinder wind turbine power generation,[3,4] and disable power lines.[5,6] A very common mechanism of icing in cold climates and seasons is associated with supercooled water droplets solidifying upon contact with surfaces. Such conditions are encountered by aircraft inside clouds[7] and by ground materials ranging from equipment to garments exposed to freezing rain.[8,9] Supercooled water is a metastable liquid phase existing practically always at subfreezing temperatures that may solidify spontaneously without (homogeneous nucleation) or with (heterogeneous nucleation) an external nucleation seed.[10] Moreover, supercooled water undergoes a 3−4-fold increase in viscosity at −15 °C relative to ambient temperature.[11] Both the metastable nature and high viscosity make repelling supercooled water rather unique and much more difficult than in the ambient case.[12−14]

Due to their excellent performance in terms of droplet repellency under ambient conditions, superhydrophobic surfaces have gained attention as a passive technique to mitigate ice accretion.[15−17] Generally, such surfaces consist of an array of microtextured features decorated with nanotexture that are coated with a conformal hydrophobic layer. They are characterized by high droplet mobility due to the presence of an intervening air layer. Furthermore, they can aid icephobicity through rapidly repelling supercooled droplets,[12,18−20] minimization of droplet−substrate heat transfer,[21,22] nucleation delay enhancement,[23,24] ice adhesion reduction,[25,26] and facile defrosting.[18,27] For droplet removal, icephobicity depends on maintaining the intervening air layer; when the intervening air layer is displaced, the so-called Cassie−Baxter-to-Wenzel wetting transition results.[28,29] In this case, the droplet sticks on the surface, resulting eventually in freezing. The ability of the texture to prevent the Cassie−Baxter-to-Wenzel transition is associated with its impalement resistance and quantified by the threshold impact velocity at which the transition takes place.

Beyond the air layer displacement, droplet mobility loss on superhydrophobic surfaces can also occur when the liquid viscosity is too high.[30,31] To underpin this statement, droplet mobility loss due to high viscosity has even been reported for

Received: April 25, 2017
Revised: June 13, 2017
Published: June 13, 2017

DOI: 10.1021/acs.langmuir.7b01412
Langmuir 2017, 33, 6708−6718

sublimating surfaces, where impalement is not an issue.[32] Likewise, we expect droplet mobility loss to occur at the onset of rapid recalescent freezing, whereby a solid−liquid slurry mixture is generated[10] and the excess droplet surface energy cannot be efficiently rectified back into kinetic energy.[18] However, to date, solidification during impact of supercooled droplets under isothermal conditions in the presence of realistic ice seeds has not been sufficiently explored; droplet icing has been achieved either because of significant substrate cooling compared to the droplet[13,18] (substrate temperatures lower than −25 °C) or after prolonged exposure to supercooled water streams.[24,33] For real-life applications, in spite of the rationally designed surface texture and chemistry that can be used to inhibit nucleation, contamination of the surface may provoke nucleation even at low levels of supercooling.

Recently, substrate flexibility—which is a property of many natural and synthetic hydrophobic materials—was shown to have a collaborative effect with existing hydrophobic micro/nanotexture on enhancing superhydrophobicity as defined by a rise in the impalement resistance[34] and a reduction in the droplet−surface contact time.[34,35] However, for flexible materials, it is unclear how viscosity and solidification affect droplet−substrate impact behavior. Such fundamental understanding is important for the rational design of icephobic surfaces. Here we show that substrate flexibility and hierarchical hydrophobic surface texture can work collaboratively toward enhancing the mobility[16] of impacting liquid droplets (boosting icephobicity and amphiphobicity[30]), as defined by the contact time (t_c) and the impalement resistance, with a range of dynamic viscosities (μ = 0.9−1078 mPa·s) and degrees of solidification (ϕ = 0−0.2), many of which are impossible for rigid materials. Droplet−substrate contact time reduction, so-called "pancake bouncing",[36] is demonstrated for a range of liquid viscosities, which can render other techniques ineffective.[37] To interpret the above behavior and facilitate the development of icephobicity and amphiphobicity design rules, we develop models based upon energy conservation considerations for predicting viscous and ice slurry droplet rebound and contact time reduction from flexible substrates on the basis of the substrate mass and stiffness. Furthermore, we investigate the effect of contamination (nucleation-promoting seeds) on supercooled droplet impact behavior and define a threshold nucleation rate based upon droplet supercooling, the surface composition, and the degree of contamination, above which the freezing dynamics are faster than the recoil dynamics. We then show that, in spite of the instantaneous freezing that occurs, the potential energy stored in the elastic substrate is able to be rectified into outgoing droplet kinetic energy and the partially solidified droplet can be ejected from the surface, overcoming adhesion, viscous, and gravitational forces. This represents an unexplored and important corollary mechanism to icephobicity, the self-cleaning of nucleating particles from surfaces with solidifying water.

EXPERIMENTAL SECTION

Materials. We obtained the following chemicals from Sigma-Aldrich: poly(methyl methacrylate) (PMMA) powder (crystalline, $M_w \approx 996000$), poly(vinylidene fluoride) (PVDF) pellets ($M_w \approx 71000$), surface-modified nanoclay (0.5−5 wt % (3-aminopropyl)-triethoxysilane, 15−35 wt % octadecylamine), silica (SiO_2) nanopowder (primary particle size 12 nm), silver iodide (AgI; 99%), *N*-methyl-2-pyrrolidone (NMP; 99.5 wt %), acetic acid (≥99.7 wt %), hydrochloric acid (37 wt %), and glycerol (≥99.5 wt %). We acquired the fluoroacrylic copolymer (PMC; 20 wt % in water, Capstone ST-100) from DuPont. We obtained the hydrophobic fumed silica (HFS; Aerosil R 8200) from Evonik, acetone (≥99.5 wt %) and isopropyl alcohol (IPA; ≥99.5 wt %) from Thommen-Furler AG, and hydrogen peroxide (30 wt %) from VWR. We purchased low-density polyethylene (LDPE) food packing film with a thickness of 12.5 μm from a local supplier.

Dispersion Preparation. We used two hydrophobic nanocomposite coatings in this work, one with low impalement resistance (nC1) and one with high impalement resistance (nC2). The coatings consisted of a fluorinated polymer, to achieve low surface energy, and nanoparticles, to increase the surface roughness. A detailed list of the ingredients and their concentrations is given in Table 1.

Table 1. Composition of Hydrophobic Coatings

ingredient	nC1 concn, wt %	nC2 concn, wt %	ingredient	nC1 concn, wt %	nC2 concn, wt %
PVDF	0.5	0.0	SiO_2	0.0	1.5
PMMA	0.3	0.0	NMP	4.3	0.0
PMC	0.0	1.4	acetone	89.5	80.2
nanoclay	4.3	0.0	acetic acid	0.0	11.0
HFS	1.1	0.0	water	0.0	5.9

For the coating nC1, we prepared stock solutions of 10 wt % PVDF in NMP and 10 wt % PMMA in acetone separately by dissolving the polymers under slow mechanical mixing overnight at 50 °C and at room temperature, respectively. We mixed 400 mg of nanoclay platelets and 100 mg of HFS in 8000 mg of acetone in a 10 mL vial, and we treated the mixture with a probe sonication (130 W, 3 mm probe, 60% amplitude, 20 kHz frequency, Sonics Vibracell, VCX-130) for 30 s. Once a stable suspension was formed, we added 440 mg of 10 wt % PVDF and 250 mg of 10 wt % PMMA, and we stirred the resulting mixture mechanically at room temperature for about 1 min.

For the coating nC2,[38,39] we suspended 140 mg of SiO_2 particles in a mixture of 600 mg of acetic acid and 4000 mg of acetone in a 10 mL vial, and we sonicated the mixture for 6 min. In a separate 10 mL vial, we mixed 500 mg of acetic acid with 4000 mg of acetone, and subsequently, we added dropwise 730 mg of 20 wt % PMC with magnetic stirring at 650 rpm. The nanoparticle suspension was added to the polymer solution with magnetic stirring at 1000 rpm.

Surface Characterization. Flexible superhydrophobic surfaces were generated by spray coating polymer−nanoparticle dispersions onto LDPE films (thickness 12.5 μm). We deposited the dispersion on the films with an airbrush (Paasche VL, 0.73 mm head) using compressed air at 2 bar at a fixed distance of ∼10 cm. We dried the samples in the oven at 90 °C for 30 min to remove any remaining solvent.

To characterize the coating wettability, we used a contact angle goniometer (OCA 35, Dataphysics Instruments) to measure the advancing (θ_a) and receding (θ_r) contact angles and the droplet sliding angle (α) by the tilting cradle method. For each measurement, we gently deposited a 6 μL droplet on the coating, which had been placed on a motorized tilting stage with graduation accuracy of 0.1 deg. The stage was inclined at 0.3 deg·s^{-1} while a digital camera acquired images of the droplet. Dedicated software (SCA202, Dataphysics Instruments) extracted θ_a and θ_r values from the images, in the front and the back of the droplet, respectively, just before the droplet started to move. We defined α as the minimum inclination angle at which the droplet started sliding. We repeated each experiment at five different spots of each coating using water, glycerol, and water−glycerol mixtures. Additionally, the same setup and software can be used for calculating the surface energy of liquids using the pendant droplet technique.

Furthermore, we characterized the coating morphology using a dark-field optical microscope (BX 60, Olympus) equipped with a digital camera (SC 50, Olympus). The measured values for θ_a, θ_r, and α along with representative micrographs for the two coatings are shown in Figure S1 (Supporting Information). The wetting character-

DOI: 10.1021/acs.langmuir.7b01412
Langmuir 2017, 33, 6708−6718

istics for nC1 and nC2 are similar and almost independent of the presence of glycerol.

Droplet Impact: Ambient Temperature. We investigated the effect of the viscosity (μ), ranging from 0.9 to 1078 mPa·s, on the droplet−substrate impact dynamics by using water and different concentrations of water−glycerol mixtures at ambient conditions (~23 °C and ~45% relative humidity). We produced droplets of almost constant diameter (D_0 = 2.1−2.4 mm) from calibrated needles with a repeatability error of less than 6% and released them from different heights to vary the impact velocity (U_0; direction normal to the surface) and the Weber number, $We = \rho D_0 U_0^2/\sigma$, where ρ and σ are the fluid density and surface tension, respectively. We use the Ohnesorge number, $Oh = \mu/\sqrt{\rho\sigma D_0} = \sqrt{We}/Re$, to relate the fluid viscosity to its inertia and surface tension, where $Re = \rho D_0 U_0/\mu$ is the Reynolds number. The water−glycerol mixture properties have been previously reported for a wide range of temperatures and concentrations.[40,41]

For all the experiments, we sectioned the flexible substrates (30 mm × 12 mm) and suspended them by mounting their shorter edge on posts. One post is stationary, whereas the other is mounted on a linear stage and can be moved. This way the strain applied on the film can be precisely controlled (see Figure S2a, Supporting Information). For the reference case, we attached the samples on a glass slide with a double adhesive tape, producing a rigid substrate. The impact events were recorded by a high-speed camera (Phantom V9.1, Vision Research) with a frame rate of 4600 s^{-1} using a back-illuminated configuration. A detailed description of the experimental setup can be found elsewhere.[34]

We assessed two different aspects of altering droplet mobility through substrate flexibility: the impalement resistance and the contact time t_c. In the first case, we impacted droplets with varying values of *We* onto the surfaces, starting from $We \approx 2$ and increasing until we observed droplet mobility loss. We used the low-impalement-resistance coating (nC1) to avoid the effects associated with elevated droplet impact velocities (splash). We mounted the flexible substrates without strain, allowing for minimum stiffness and a marked effect of flexibility on impalement resistance.[34] We recorded three possible wetting states from each impact event: (a) total rebound, when the droplet recoiled from the surface, leaving no liquid behind; (b) partial rebound, when part of the droplet recoiled from the surface while the other portion remained attached; (c) no rebound, when the droplet was unable to recoil from the surface. For hierarchical random surface textures, such as the ones used in this study, the manifestation of the different wetting states is of stochastic nature due to multiple transitioning states (micro- and nano-Cassie).[29,42] In other words, to characterize such behavior, one should use the same impact conditions and measure the probability of observing each impact outcome, which we denote by Φ_r for total rebound, Φ_p for partial rebound, and Φ_n for no rebound.[34] Consequently, for each *We* and *Oh* combination, we tested five different LDPE samples and impacted each sample three times at the same spot, gathering in total fifteen measurements. Then we measured the occurrence of each outcome and divided by the total number of measurements to estimate Φ_r, Φ_p, and Φ_n.

To study the effect of μ and the degree of solidification (ϕ) on t_c, we used samples coated with the high-impalement-resistance coating (nC2). The setup configuration and sample dimensions were kept the same as before, but for these experiments, the flexible samples were fixed with ~0.5% strain. This amount of strain is suitable for observing reduction in t_c without stretching considerably the superhydrophobic coating.[34] We used water, glycerol, and three water−glycerol mixtures, producing a range of *Oh* that spanned 3 orders of magnitude (from 2.2 × 10^{-3} to 2.6). It has been proposed that t_c reduction takes place only if the *We* is above a threshold value,[35] which we denote by We_c. To determine We_c for a given *Oh*, we started by selecting two values of *We* at the extreme ends of our search range. One value was sufficiently low that normal rebound always occurred, and one was sufficiently high that t_c reduction was always observed. Then we used an iterative bisection method,[43] where at each iteration we test the intermediate *We*, and we updated the search space accordingly. For each value of *We*, we repeated the droplet−substrate impact experiment five times. We terminated the procedure either if the search space was confined enough or if we acquired inconsistent results on the five repetitions.

Droplet Impact: Subfreezing Temperature. We performed droplet−substrate impact experiments at subfreezing environmental temperatures. The environment, substrate, and droplet temperature were controlled with an insulated chamber cooled by a constant supply of dry vapor produced by boiling liquid nitrogen (see Figure S2b, Supporting Information). We investigated the effect of flexibility on t_c for temperatures ranging from +15 to −15 °C using the same coatings and sample support as in the ambient temperature experiments. We note at this point that imposing an accurate and uniform strain on the flexible substrate was not possible in this setup due to space restriction. The droplet impact experiments were performed under quasi-isothermal conditions. The temperature difference between the substrate and the droplet was kept below 4 °C. The reported droplet temperatures (T_d) have been corrected to account for evaporation due to the dry nitrogen environment; the calibration for the correction and a detailed description of the insulated chamber can be found in ref 12. The properties of supercooled water have been documented in previous studies.[11,44,45]

Finally, we impacted supercooled water droplets on artificially contaminated by design flexible and rigid substrates. We impacted each droplet onto a different spot on the surface to ensure that the level of contamination was kept the same. All impacts were recorded with the same high-speed camera and configuration as in the ambient temperature experiments.

Artificial Contamination. As a contaminant, we selected AgI particles, which are a known ice nucleation promoter.[46] To control the degree of surface contamination, we used the following procedure. For low-level contamination, we cleaned glass microscopy coverslips by treating them for 7 min with a piranha solution (1:2 solution of hydrogen peroxide in hydrochloric acid), followed by bath sonication for 1 min in acetone and 1 min in isopropyl alcohol. Finally, we moved and stored the sample in deionized water until use. We prepared dispersions of AgI in acetone with different concentrations. The dispersions were treated with probe sonication for 1 min. We placed sections of the LDPE film coated with the nC2 coating on microscopy glass slides alongside the clean coverslips, after drying them under a nitrogen flow. We sprayed the AgI dispersion on both the sample and the coverslip using an airbrush while keeping the substrate temperature at 50 °C. Since AgI does not form a stable dispersion in acetone and precipitates relatively fast, we took special care to mechanically stir the mixture just before the spaying procedure. Micrographs of the coverslip were acquired for five random spots before and after the artificial contamination to assess the degree of surface coverage (ψ_c) by the AgI particles. We define ψ_c as the difference between the portions of the area covered by particles before and after the contamination. For high-level contamination, we sprinkled the AgI particles on the sample using a sieve until the surface turned yellow and tilted the sample more than 90° to eliminate possible pileups. In these cases, we assumed that every part of the droplet surface touching the substrate has a practically 100% probability to come in contact with some nucleating particle and therefore $\psi_c \approx 100\%$. Still, the actual coverage may be a little smaller since the substrate was not completely covered with AgI particles.

Statistical and Error Analysis. For all values reported, we estimated the mean value and the 95% confidence interval (CI) of the mean from the collected measurements. Moreover, we calculated the theoretical propagated measurement error, given the accuracy of our measuring equipment. We assume that if the CI is greater than the propagated measurement error, then the latter is contained in the CI. In the following, we report either the CI interval or the propagated measurement error, whichever is greater, trying to capture both effects emerging from the independent experiments and the measurement equipment. The sample size (n, number of independent experiments) and the total number of experiments (n', sum of replications for all independent experiments) are reported in the legend of each figure, wherever applicable. Finally, we report the 95% confidence interval of

DOI: 10.1021/acs.langmuir.7b01412
Langmuir 2017, 33, 6708−6718

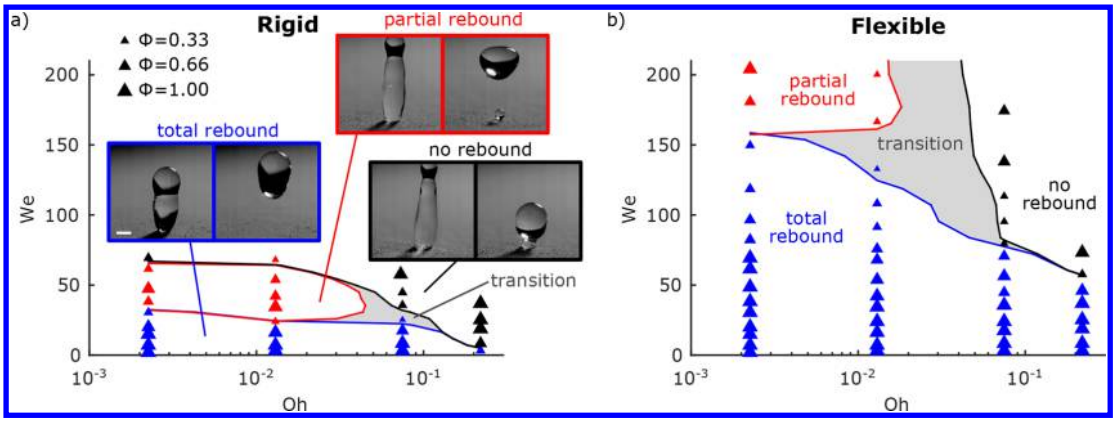

Figure 1. Effect of the droplet viscosity on the rebound behavior of droplets impacting flexible and rigid superhydrophobic substrates. Droplet−substrate impact outcome vs *We* and *Oh* for (a) rigid and (b) flexible substrates (D_0 = 2.1−2.4 mm). Symbols represent the highest probability of a given outcome: "total rebound" (Φ_r = max(Φ_r,Φ_p,Φ_n), blue triangles), "partial rebound" (Φ_p = max(Φ_r,Φ_p,Φ_n), red triangles), and "no rebound" (Φ_n = max(Φ_r,Φ_p,Φ_n), black triangles). The surface area of the triangles scales with Φ (see the legend). To vary *Oh*, various concentrations of glycerol in water were used for the droplets (0, 50, 75, and 85 wt % glycerol stated with increasing *Oh*). The sample size of independent experiments (n) is 5, and the number of total experiments (with replications, n') is 15. The substrate was treated with nC1. Lines represent approximate transitions between different impact outcomes. Shaded gray areas labeled as "transition" indicate the regions where all three outcomes were observed but none of the associated probabilities is greater than 0.5. Inset images in (a) show representative behavior for the different impact outcomes. The scale bar in (a) represents 1 mm.

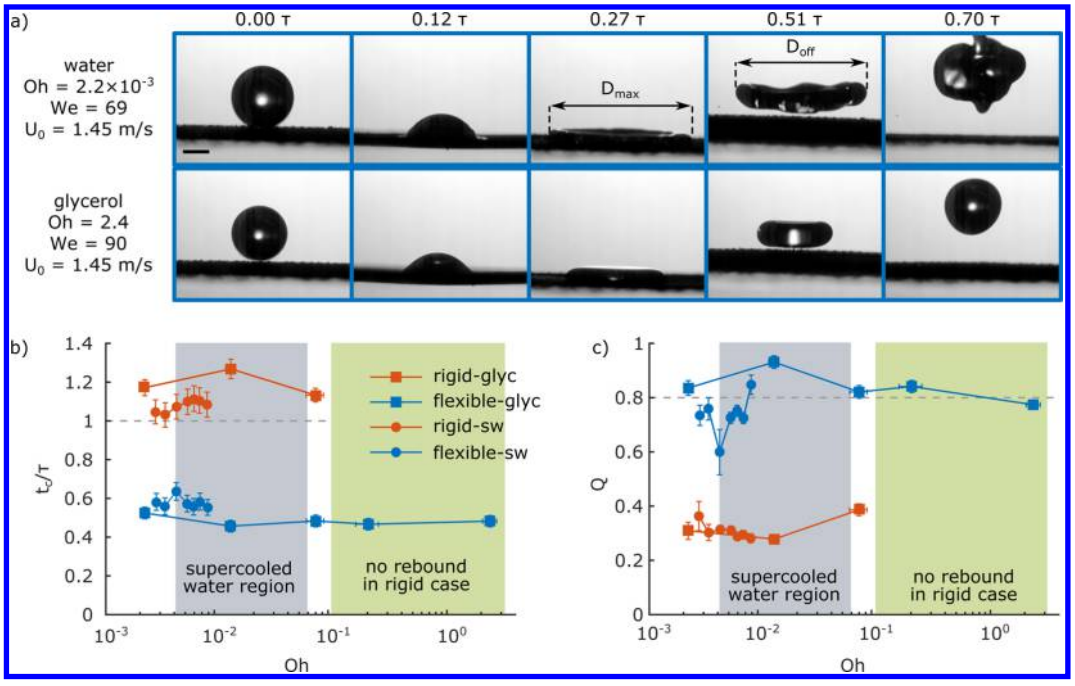

Figure 2. Effect of the droplet viscosity on the contact time reduction for droplets impacting a superhydrophobic substrate. (a) Image sequence of water (top row; properties: $Oh = 2.2 \times 10^{-3}$, $We = 69$, and $U_0 = 1.45$ m·s^{-1}) and glycerol (bottom row; properties: $Oh = 2.4$, $We = 90$, and $U_0 = 1.45$ m·s^{-1}) droplets impacting a flexible substrate coated with nC2. The maximum spreading (D_{max}) and the takeoff diameter (D_{off}) are also defined (top row). (b) Dimensionless contact time (t_c/τ) vs *Oh* for the rigid (red squares and circles) and flexible (blue squares and circles) substrates ($\tau \approx 10$ ms, D_0 = 2.2−2.4 mm). *Oh* was varied by either changing the supercooling of the water (red and blue circles, sw, $U_0 = 1.31$ m·s^{-1}, $n = 5$) or by the addition of glycerol (red and blue squares, glyc, $U_0 = 1.45$ m·s^{-1}, $n = 10$). The "gray" shaded area indicates the *Oh* range that corresponds to supercooled water with a temperature range of −1 °C to the homogeneous nucleation temperature[44] of −38 °C for D_0 = 2.2 mm. The "green" shaded area indicates the *Oh* range where we observed no droplet rebound from rigid substrates. The dashed gray line indicates the theoretical minimum[47] of t_c/τ for normal rebound of inviscid droplets impacting a rigid substrate (single oscillation of a droplet). (c) Pancake quality, $Q = D_{off}/D_{max}$, vs *Oh* for the same experiments as in panel b. The scale bar in (a) represents 1 mm.

the population, based on its standard deviation, for the reproducibility error for D_0.

RESULTS AND DISCUSSION

Droplet Mobility: Impalement Resistance. Figure 1 shows the probabilities of the different outcomes for droplet collisions on (a) rigid and (b) flexible substrates for a range of *We* and *Oh*; the color of the triangles corresponds to the outcome with the higher probability and its surface area to the respectful value (examples for each outcome are shown as insets in Figure 1a). The lines mark the transition between the different regimes, which we draw using the following procedure.

DOI: 10.1021/acs.langmuir.7b01412
Langmuir 2017, 33, 6708−6718

We assume that Φ_r, Φ_p, and Φ_n are smooth functions (surfaces) on the *We* and *Oh* plane. We used cubic smoothing splines to interpolate the surface values in the whole plane given our experimental data. The lines separating the different regions were calculated as the isolines for Φ_r, Φ_p, and $\Phi_n = 0.5$. There are regions on the *We* and *Oh* plane where we observed all of the possible outcomes, and none of the associated probabilities exceeded the value of 0.5. We shaded these regions gray in Figure 1 and labeled them as "transition".

For the flexible case, high droplet mobility is sustained for a much wider region of *We* and *Oh*. We observed an approximately 4-fold increase in the *We* where the transition from total rebound to partial rebound or no rebound takes place. We attribute this enhancement in impalement resistance—the ability of the surface texture to resist meniscus penetration—to the substrate acceleration prior to contact with the droplet,[34] an effect that is practically independent of μ. We note though that, in both the flexible and rigid cases, increasing *Oh* reduced the value of *We* where the transition from total to no rebound occurs since an increase in μ impedes recovering from partial penetration into the texture.[12] Additional information on characterizing the droplet impalement is given in the Supporting Information (section "Droplet Impalement" and Figure S3).

Droplet Mobility: Droplet–Substrate Contact Time Reduction. Additionally, droplet mobility can be enhanced by reducing the droplet–substrate contact time (t_c). Figure 2a shows an image sequence of water (top row) and glycerol (bottom row) droplets impacting a coated (superhydrophobic, nC2) flexible substrate for similar values of U_0 and τ (see also Movie S1, Supporting Information). In both cases, the droplets levitate and separate from the surface in a pancake shape, an indication of t_c reduction.[36] Figure 2b plots t_c/τ vs *Oh* for supercooled water and water–glycerol droplets impacting flexible and rigid substrates, where $\tau = (\pi/4)\sqrt{\rho D_0^3/\sigma}$ is the inertial capillary time. For liquid droplets with low viscosity, τ is equal to the theoretical period of natural oscillation of the droplet.[48] For the same substrate and coating type, we observed a good agreement between the water–glycerol and the supercooled water droplet impact experiments in terms of t_c/τ. By using flexible substrates, one can achieve a 50% reduction in t_c compared to that in the rigid case. We note that, for $Oh > 0.1$, droplets that impact rigid substrates were unable to rebound from the surface, contrasting the large t_c enhancement resulting from substrate flexibility. Additionally, Figure 2c is a plot of the "pancake" quality,[36] $Q = D_{off}/D_{max}$, vs *Oh*, where D_{max} is the droplet diameter at maximum extension and D_{off} is the diameter of the droplet when it separates from the surface. Previous work[36] suggests that $Q > 0.8$ is necessary for an impact event to be considered pancake bouncing, which we observe for water–glycerol droplet mixtures impacting superhydrophobic flexible substrates.

Figure 3a presents the rebound behavior (reduced vs normal t_c modes; representative experiments are presented in Movie S2 for water and Movie S3 for glycerol) for a range of *We* and *Oh*. It also plots We_c vs *Oh* where the transition between the two rebound modes takes place. For $We < We_c$, the droplet rebound resembles that observed for rigid surfaces with low-viscosity liquids; the droplet retracts and uses the stored surface energy to recoil with a t_c that is comparable to τ. This is in accordance with previous reports for water droplet–substrate impacts on elastic superhydrophobic substrates.[35] For viscous droplets

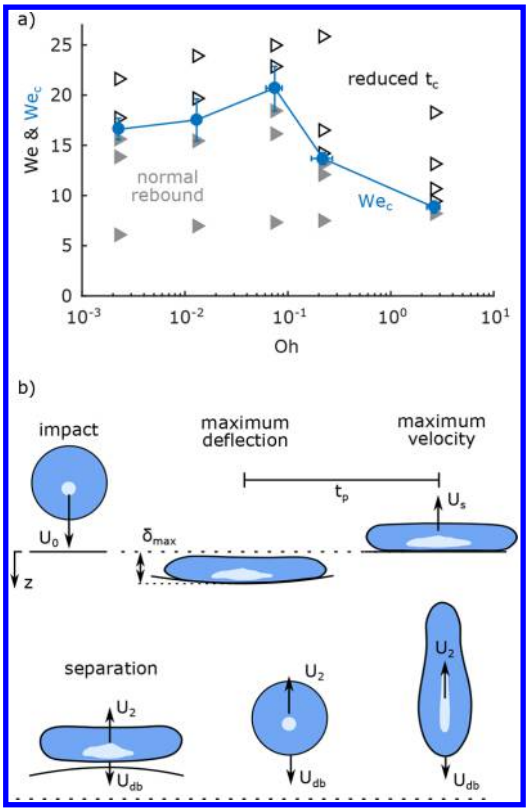

Figure 3. Mechanism of viscous droplet–substrate contact time reduction. (a) Experimental rebound behavior vs *We* and *Oh*: reduced (open right-pointing triangles) vs normal (solid right-pointing triangles) t_c for $D_0 = 2.1$–2.4 mm. We also plotted We_c vs *Oh* (blue line and circles), with the vertical error bars denoting the span from the highest tested value where normal rebound was detected to the lowest value which resulted in reduced t_c. The sample size (n) is five repetitions per point. (b) Schematic showing the relevant stages during droplet impact and early rebound (just before impact, at substrate maximum deflection, at substrate maximum velocity, at the point of separation, and oscillating airborne from left to right). The droplet has a velocity U_s when it passes the point $z = 0$ for the second time. After separation, the droplet center-of-mass moves with velocity U_2, while its base has a relative velocity U_{db}.

impacting the flexible substrates, the rebound mode for $We < We_c$ resembles that described before (water impacting rigid substrates; see Movies S2 and S3, Supporting Information, for comparison), even though we did not observe rebound in the rigid case. To explore the limit of our flexible surfaces, we impacted an ultraviscous and sticky liquid, namely, honey (17 wt % water content). The values $\rho = 1472$ kg·m^{-3} and $\mu = 22.55$ Pa·s were taken from the literature,[49] and $\sigma = 76.8 \pm 1.8$ mN·mm^{-1} was measured using the pendant droplet technique (see the Experimental Section). For $D_0 \approx 2.8$ mm, we determined experimentally that $We_c = 18 \pm 10$ using the same procedure as before. In this case, the droplets impacting with $We < We_c$ were unable to rebound and remain stuck on the surface, whereas for $We > We_c$ we observed rebound (see Figure S5 and Movie S4, Supporting Information). In the following, we characterize the substrate behavior upon impact, and we employ a scaling analysis based on energy conservation to predict the onset of t_c reduction and rationalize our results.

LDPE Film Energy Rectification. To quantify the role of the film on the droplet rebound, we extended the set of our experiments with droplet impact using $D_0 = 1.8$ to 2.9 mm for

DOI: 10.1021/acs.langmuir.7b01412
Langmuir 2017, 33, 6708–6718

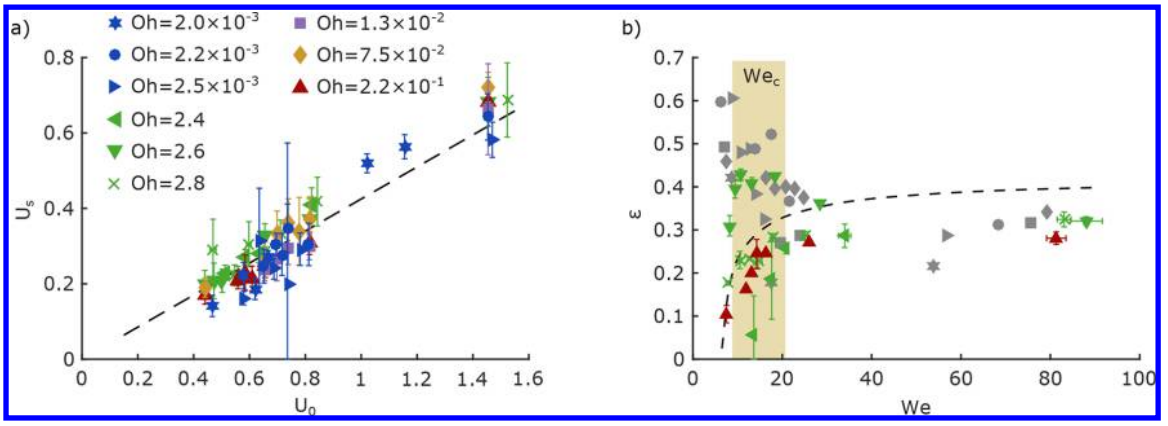

Figure 4. LDPE film ability to rectify energy. (a) Droplet−substrate velocity after impact (U_s) vs impact velocity (U_0) for different *Oh* values (water D_0 = 2.9 mm, water D_0 = 2.4 mm, water D_0 = 1.9 mm, 50 wt % glycerol D_0 = 2.2 mm, 75 wt % glycerol D_0 = 2.1 mm, 85 wt % glycerol D_0 = 2.1 mm, glycerol D_0 = 2.6 mm, glycerol D_0 = 2.1 mm, and glycerol D_0 = 1.8 mm stated with increasing *Oh*). The dashed line represents the linear fit (slope 0.425). The sample size (n) is five repetitions per point. (b) Coefficient of restitution (ε) vs *We* for the same experiments as in panel a. Colored points correspond to mixtures with *Oh* > 0.1 that would not normally rebound from a rigid surface and gray points to mixtures with *Oh* < 0.1. Markers as in panel a. The theoretical prediction (eq 2) is shown by the dashed line. The shaded area marks the *We* region where the transition to pancaking occurs. The sample size (n) is five repetitions per point.

water and glycerol. We measured the maximum deflection of the substrate after impact (δ_{max}) and the time (t_p) needed for the droplet−substrate system to travel from δ_{max} to its initial undisturbed position (z = 0; see Figure 3b for definition). We assume that the droplet−substrate system oscillates harmonically during this time, that is, $\delta = \delta_{max}\cos(\omega_s t + d)$, where δ is the substrate deflection at time t, $\omega_s \approx \pi/(2t_p)$ is the angular velocity of the oscillation, and d is an initial phase. Here, we neglect the energy losses in the substrate for simplicity, but as we see later this assumption does not induce a serious error. As a result, the amplitude of the velocity during the oscillation is $U_s \approx \delta_{max}\pi/(2t_p)$ (see Figure 3b for the definition of U_s).

Figure 4a plots experimental values of U_s vs U_0 and exposes a linear trend between the two. It is then useful to introduce the rectification coefficient, $c_u = U_s/U_0$, which captures the portion of momentum the droplet has during the droplet−substrate oscillation in comparison to that before impact. We estimated c_u = 0.425 by weighted linear least-squares fitting (dashed line in Figure 4a). Notably, the mass of the impacting droplet has no effect on U_s. This behavior can be interpreted by idealizing the droplet−substrate system as a mass oscillating by two springs connected in series, one arising from the droplet deformability (k_d) and one from the film stiffness (k_f). Here, we assume that the film mass is negligible. If additionally the ratio of the film and droplet stiffness is constant, then the film will absorb and rectify a constant portion of the total energy of the system, that is, $c_u^2 = k_d/(k_d + k_f)$. Hence, the film converts a fraction of the droplet kinetic energy ($E_{k,0} = \pi D_0^3 \rho U_0^2/12$) as elastic strain energy (which scales with δ_{max}^2), resulting in $\delta_{max} \propto \rho^{0.5} D_0^{1.5} U_0$. For the oscillating system, since the mass comes from the droplet, the angular velocity of the droplet−substrate system is proportional as $\omega_s \propto \rho^{-0.5} D_0^{-1.5}$. By multiplying these terms, $U_s = \delta_{max}\omega_s \propto U_0$, the effect of the droplet mass on U_s vanishes and it is only dependent on U_0. In other words, heavier droplets will deflect the substrate more, but the oscillation will take place at a lower frequency. In general, when the droplet mass is much greater than the effective mass of the substrate, c_u is related to the relative stiffness between the substrate and droplet. If the substrate mass is not negligible, then the ratio of the substrate to the droplet mass defines δ_{max} through an inelastic collision model[50,51] and therefore c_u.

To further support this assumption, we measured the velocity of the droplet after separation (U_2), which is equal to U_s reduced by the energy needed to separate the droplet from the surface. This energy is defined as the practical work of adhesion:

$$W_{ad} \approx \frac{\pi D_{max}^2}{4}\sigma(1 + \cos\theta_r) \quad (1)$$

We measured U_2 by tracking the droplet centroid in our image sequences and fit a parabolic trajectory. For low *Oh*, the droplets contacted the substrate for a second time after the initial separation, so we took care to estimate U_2 using only the frames in between. The kinetic energy of the droplet after separation is $E_{k,2} = E_{k,1} - W_{ad}$, where $E_{k,1} \approx \pi D_0^3 \rho U_s^2/12 \propto c_u^2 U_0^2$. In terms of the coefficient of restitution, $\varepsilon = U_2/U_0$, $\varepsilon^2 \approx c_u^2 - 3\xi^2(1 + \cos\theta_r)/We$, where $\xi = D_{max}/D_0$ is the spreading parameter. Since for *Oh* > 0.1 the droplets do not rebound from the rigid substrate, we assume that, independent of the outcome, either reduced t_c or normal rebound, U_2 is attributed solely to the substrate action. For highly viscous fluids, $\xi \approx b_v Re^{0.2}$, where b_v is the scaling factor between the ξ and $Re^{0.2}$ (see the Supporting Information, section "Maximum Spreading"); therefore

$$\varepsilon = \sqrt{c_u^2 - \frac{3b_v^2(1 + \cos\theta_r)}{We^{0.8}Oh^{0.4}}} \quad (2)$$

We plot eq 2 using the values for glycerol (θ_r = 141° and *Oh* = 2.6) in Figure 4b, along with the experimentally measured values for ε. For better inspection, the values for fluids with *Oh* > 0.1 are plotted in color and the rest are shown in gray. The predicted curve captures the experimental trend while slightly overestimating ε, most likely due to the neglected energy losses on the film, but still the error is relatively small. In the case of *Oh* < 0.1, the droplet stores surface energy, which is released during its retraction. For *We* lower or close to We_c, part of this energy assists the droplet in achieving a higher U_2, which is reflected by the deviation of ε toward higher values. As t_c reduction takes place, the value of ε converges for all *Oh* to a constant value.

DOI: 10.1021/acs.langmuir.7b01412
Langmuir 2017, 33, 6708−6718

Energy Balance for Contact Time Reduction. In our experiments, we observed that, for highly viscous droplets, which are unable to recoil after impacting rigid substrates, the rebound mode on flexible substrates shifts from reduced t_c to normal with decreasing We (see Movie S3, Supporting Information). Accordingly, $E_{k,2}$ in this case allows for droplet rebound but not for t_c reduction. We hypothesize that, as the droplet is close to the separation point, it still oscillates, and such oscillations can hinder the droplet rebound in a pancake shape; therefore, one should eject the droplet fast enough that the droplet oscillation is decoupled from the recoil dynamics (see Figure 3b). Hence, we are motivated to introduce a minimum of excess kinetic energy needed for t_c reduction, which we denote in the following as $E_{k,ex}$. Moreover, gravity does not play an important role in the process; for a rigid body in contact with an oscillating elastic substrate, separation will occur if the acceleration due to the oscillation will surpass the gravitational acceleration (g), or stated mathematically $\omega_s U_s > g$. Typical values for ω_s are on the order of 500 rad·s^{-1}, allowing for separation even at U_s on the order of 0.01 m·s^{-1}. This value is well below the U_2 which we recorded on the onset of t_c reduction in our experiments.

We speculate that $E_{k,ex}$ is connected to the retraction velocity of the droplet. The retraction of the droplet pushes its base toward the surface, counteracting the droplet−substrate separation. To estimate the $E_{k,ex}$, we assume that just before separation the base of the droplet moves with a velocity of $U_2 - U_{db}$, where U_{db} is the downward velocity of the base in a frame moving with the droplet (see Figure 3b). We expect U_{db} to be proportional to the retraction rate of the droplet, which scales as D_{max}/τ_r, where τ_r is equal to τ for inertia-dominated retraction and to the viscous relaxation time, $\tau_v = \mu D_0/\sigma$, for viscosity-dominated retraction.[52] The proposed crossover between the two regimes has been placed at $Oh = 0.05$,[52] but in our experiments values closer to $Oh \approx 1$ seem to be a better choice (for example, τ_v is 3.5 times smaller than τ at $Oh \approx 0.22$, resulting in an overestimation of the retraction rate). Accordingly, to overcome the effect of droplet retraction, $E_{k,ex} \sim \pi D_0^3 \rho U_{db}^2/12 \sim (\pi D_0^3 \rho/12)(D_{max}/\tau_r)^2$, and in a normalized form, $E_{k,ex}/E_{k,1} \sim (\xi\tau)^2/(c_u^2 We \tau_r^2)$. In the same manner, we normalize the practical work of adhesion, $W_{ad}/E_{k,1} \approx 3\xi^2(1 + \cos\theta_r)/(c_u^2 We)$. For any given fluid, we observe that the total energy resisting the t_c reduction is $(W_{ad} + E_{k,ex})/E_{k,1} \sim \xi^2/We$, which motivates the introduction of an early jumping parameter, $P_j = \xi/\sqrt{We}$. Figure 5 plots the experimental values for P_j at the onset of t_c reduction vs Oh. We define a critical value ($P_{j,c}$) to predict a type of rebound; for $P_j > P_{j,c}$, normal or no droplet rebound is expected, whereas, for $P_j < P_{j,c}$, reduced t_c bouncing is expected. The theoretical value for $P_{j,c}$, given the relations for W_{ad} and $E_{k,ex}$, is

$$P_{j,c} \approx \frac{c_u}{\sqrt{3(1 + \cos\theta_r) + c_r(\tau/\tau_r)^2}} \tag{3}$$

where c_r is the numerical coefficient connecting $E_{k,ex}$ to $(\pi D_0^3 \rho/12)(D_{max}/\tau_r)^2$. The calculation of $P_{j,c}$ takes into account the surface wettability, the ability of the substrate to rectify the elastic strain energy to the droplet, and the liquid properties. We identify two limiting cases: (a) at the low-viscosity limit, e.g., for water, where $\xi \approx b_c We^{0.25}$ and $\tau/\tau_r = 1$ and (b) at the high-viscosity limit, e.g., for glycerol, where $\xi \approx b_v Re^{0.2}$ and $\tau/\tau_r = \pi/(4Oh)$ (see the Supporting Information, section "Maximum Spreading", for more on the spreading dynamics on flexible substrates), where b_c and b_v are proportionality coefficients.[53] At the low-Oh regime, the value of $P_{j,c}$ is independent of the liquid properties

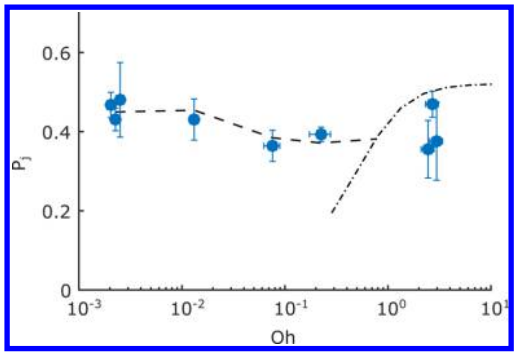

Figure 5. Jumping parameter (P_j) for the flexible substrates. P_j at the onset of t_c reduction vs Oh (same points denoted by We_c in Figure 3a, including points with D_0 = 1.9 and 2.9 mm for water droplets and D_0 = 1.8 and 2.6 mm for glycerol). Low-viscosity (---, eq 4) and high-viscosity (-·-, eq 5) theoretical values for the critical jumping parameter ($P_{j,c}$), below which reduced contact time is expected.

$$P_{j,c} \approx \frac{c_u}{\sqrt{3(1 + \cos\theta_r) + c_r}} \tag{4}$$

and $We_c = (bc/P_{j,c})^4$. On the contrary, at the high-Oh regime

$$P_{j,c} \approx \frac{c_u}{\sqrt{3(1 + \cos\theta_r) + (\pi^2/16)c_r Oh^{-2}}} \tag{5}$$

which results in lower values for We_c with increasing Oh. We solve for the value of We_c as

$$We_c = Oh^{-0.5}\left(\frac{b_v}{c_u}\right)^{2.5}\left[3(1 + \cos\theta_r) + \frac{\pi^2}{16}c_r Oh^{-2}\right]^{1.25} \tag{6}$$

We plot the theoretical values for $P_{j,c}$ using the measured values for θ_r and $c_r = 0.51$ for the whole range of Oh in Figure 5. The equation for viscosity-dominated retraction is employed above $Oh > 1$. Good agreement between the theoretical and measured values is observed.

We also note that, in the case of honey, we expect $E_{k,ex} = 0$, and thus, W_{ad} is the only factor impeding the rebound. On the basis of the measured $\theta_r = 142 \pm 10°$ and $\alpha = 3.6 \pm 1.7°$ for 12 μL honey droplets, we calculated a value for W_{ad} based on the contact diameter 14 times lower than that estimated by balancing $E_{k,1}$ at We_c. This discrepancy most likely arises from the fact that calculation of W_{ad} does not capture the complex mechanism involved in the dewetting of such a liquid. The creation and disruption of capillary bridges on the texture asperities[54] and viscous dissipation[55] may increase W_{ad}. The non-Newtonian nature of honey[49] can also impede its dewetting.[56]

The reduction in t_c and the repellency of highly viscous fluids by flexible substrates are based on the ability of the substrate to absorb $E_{k,0}$ and rectify it back to the droplet, aiding separation. Additionally, the timing of the energy rectification is an important factor; the droplet−substrate system should oscillate sufficiently fast for the droplet to recoil earlier in time. We detected separation for the droplet−substrate system at the highest point of its oscillation, namely, at time $\sim 3\pi/(2\omega_s)$ after impact. Thus, the expected $t_c/\tau \approx 3\pi/(2\omega_s\tau)$, which results in ~0.5 for the typical values of ω_s and τ from our experiments and matches well with the observed one. For highly viscous

DOI: 10.1021/acs.langmuir.7b01412
Langmuir 2017, 33, 6708−6718

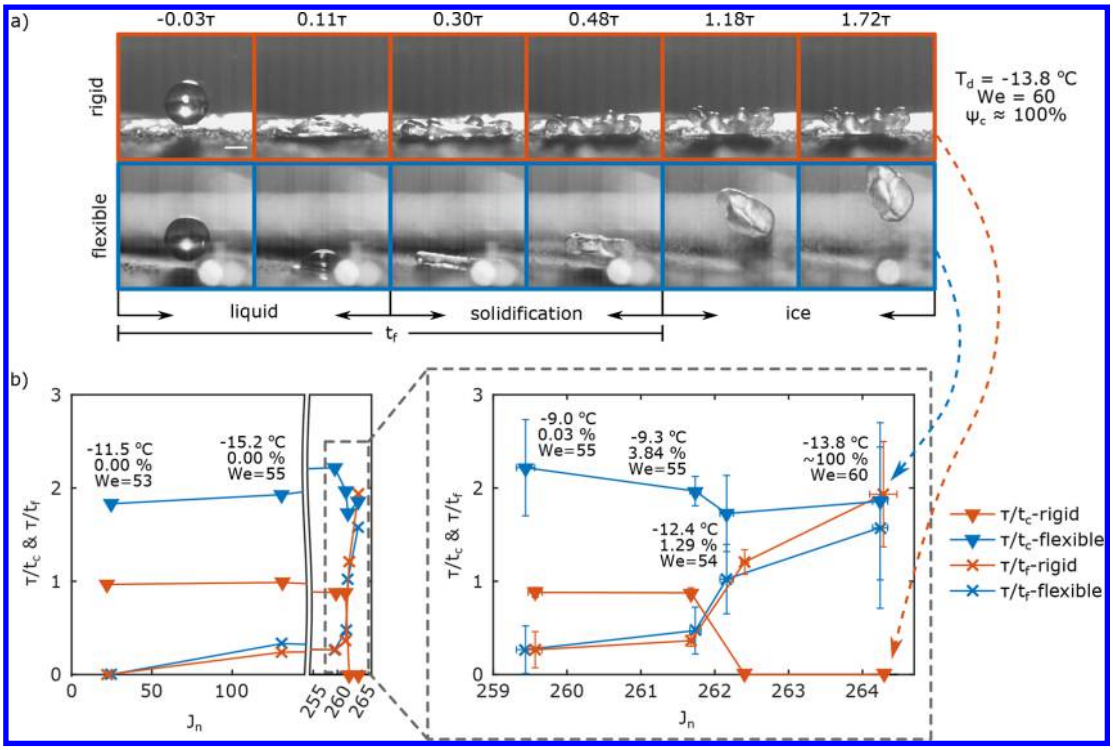

Figure 6. Role of flexibility in repelling partially solidified droplets. (a) Snapshot of a supercooled droplet impacting flexible and rigid substrates contaminated with AgI particles ($\psi_c \approx 100\%$, $D_0 = 2.0$ mm, $We = 60$, $T_d = -13.8$ °C). (b) Rebound (τ/t_c) and recalescence (τ/t_f) solidification rates vs the normalized nucleation rate (J_n) for rigid and flexible substrates ($D_0 = 2.0-2.4$ mm, $We = 53-60$, $\psi_c = 0-100\%$, and T_d from −9 to −15 °C). Also enlarged is the region where $\tau/t_f \approx \tau/t_c$. Rates with zero value indicate an absence of the respective event, either no rebound or no solidification. Next to each point for the flexible case, the T_d, ψ_c, and We are indicated, from top to bottom, respectively. For the rigid case, the impact and contamination conditions are similar to those reported for the flexible case for similar values of J_n. Error bars are omitted in the left panel for better inspection. The sample size (n) is 4−5 repetitions per point. The scale bar in (a) represents 1 mm.

liquids that do not recoil from the rigid surface, these timing considerations are irrelevant.

Contact time reduction on elastic substrates has been previously connected to splashing, with gravity opposing its manifestation.[35] As we explained previously, gravity plays a minor role in the dynamics of the substrate-aided rebound. Moreover, the proposed Froude number criterion[35] for early droplet recoil, which connects the upward substrate inertia to gravity, $Fr = U_s/\sqrt{gD_{max}} > 1$, was valid in our experiments even for $We < We_c$, further supporting that the gravitational effect can be neglected. Most importantly, the previous model for predicting t_c reduction relates its onset with splashing, a counterintuitive connection. This implies that We_c is independent of the substrate properties, such as its ability to rectify energy, and depends solely on the surface roughness and liquid properties. Specifically, with increasing values of μ, the We_c should also increase for the splashing conditions to occur. In our experiments, we observe the opposite trend. In addition, for water, We_c is notably lower than the previously reported value for the same D_0 = 2.3 mm (around 17 in this study compared to 51) and well away from the splashing regime. In summary, the suggested mechanism in this study differs from the previously reported one, since it connects the early droplet recoil mainly to the action of the substrate and to the surface wettability, and not to the action of the air layer under the leading edge of the spreading droplet.[35]

Repellency of Solidifying Droplets. The repellency of solidlike droplets and the ability of flexible surfaces to rectify the incoming kinetic energy to outgoing kinetic energy and overcome adhesion motivate their use in repelling solidifying droplets. In the case of real-life applications, solidification of supercooled water is more likely to occur in the presence of contamination on the surface rather than as a homogeneous process, a fact that is also observed in our experiments. Briefly, on the AgI-contaminated surfaces, we always detected solidification of the impacting droplets, whereas, for clean surfaces, we detected solidification for a few impacts only at temperatures below −15 °C. On the other hand, the rate of solidification ($1/t_f$), where t_f is the time elapsed from substrate contact until the completion of the first stage of freezing,[10,57] was significantly varied. We determined the completion of the freezing process optically, by the total clouding of the droplet volume and the standstill of the droplet surface (see Figure 6a and Movie S5, Supporting Information, for definition). In accordance with theory, higher levels of subcooling and contamination (ψ_c) increased $1/t_f$. To quantify the probability of droplet solidification, we calculated the normalized rate of critical ice embryo formation (J_n) on the basis of classical nucleation theory[23,24,58] (see the Supporting Information, section "Rate of Critical Ice Embryo Formation"). The higher the value of J_n, the more likely one is to observe the nucleation of the droplet and the faster the $1/t_f$.

Snapshots of a droplet impacting a highly contaminated surface are shown in Figure 6a. The first stage of solidification is completed fast enough and is called "recalescent freezing", which takes place on the order of ∼10 ms,[10] resulting in the droplet remaining frozen almost at the point of maximum spreading. For the rigid case, rebound is completely suppressed as the excess surface energy remains stored in the partially

DOI: 10.1021/acs.langmuir.7b01412
Langmuir 2017, 33, 6708−6718

frozen droplet and is not readily available after complete freezing. On the other hand, the droplet rebounds in the flexible case, due to efficient rectification of the substrate strain energy back to outgoing droplet kinetic energy. Figure 6b shows the normalized rebound rate (τ/t_c) and solidification rate (τ/t_f) vs J_n (D_0 = 2.0−2.4 mm, We = 53−60, and T_d from −9 to −15 °C); J_n was varied via the droplet temperature and concentration of surface contamination (ψ_c). The absence of an event, either rebound or solidification, corresponds to zero for the respective rate. When $\tau/t_f < \tau/t_c$, rebound always occurs for droplets impacting both rigid and flexible substrates. This is because solidification takes place after droplet−substrate separation. If $\tau/t_f \approx \tau/t_c$, for impacts on the rigid substrates, the droplets do not rebound; the stored surface energy is not rectified back to kinetic energy, resulting in droplet arrest. The positive effect of increased τ/t_c on droplet rebound under solidifying conditions is in accordance with previous studies with macrotextured surfaces on the molten metal droplets.[47] With a further increase in τ/t_f, one would expect that the droplets would also stop rebounding from the flexible substrates as $\tau/t_f > \tau/t_c$, but this is not the case. The stored strain energy was able to overcome the water−ice slurry adhesion, and the solidifying droplets were thrown away by the surface action (examples of the collision outcome for flexible and rigid substrates for varying τ/t_f are presented in Movie S6, Supporting Information). We expect that the work of adhesion for the water−ice slurry should be greater than W_{ad}, but to our knowledge, no analytical description is available. However, we anticipate that the surface wettability should play an important role since it has been shown that W_{ad} is proportional to the strength of the ice adhesion.[25] Separately, high values of c_w, which can be tuned by the substrate stiffness, are also desirable in this case, since more energy will be available for shedding the ice−water mixture from the surface.

The repellency of solidifying droplets has a triple role in mitigating ice accretion. First, flexibility is acting both as a means for reducing t_c, lowering the probability of droplet arrest due to solidification, and as a passive ice shedding mechanism. Furthermore, the self-cleaning mechanism of superhydrophobic surfaces,[59] which is well understood at room temperature, is extended at the deeply supercooled range. The impacting droplets carry away the contaminating particles that promote ice nucleation, thus lowering the readiness of the subsequent droplet to solidify. This can be thought of as a new mechanism that promotes icephobicity.

CONCLUSION

In this work, we reported the use of substrate flexibility, working collaboratively with surface micro/nanotexture, as a passive means to repel supercooled and viscous droplets. We quantified these findings by the decline in the impalement probability, the reduction in the droplet−substrate contact time, and the increase in the droplet recoil velocity. We experimentally demonstrated these results for a range of droplet supercooling and viscosities and explained the underlying mechanisms with appropriate modeling (impalement, kinetic−capillary; substrate energy rectification and contact time reduction, kinetic−elastic−capillary). We showed that the repellency of highly viscous liquids, which do not recoil from rigid superhydrophobic substrates, is accomplished because of the efficient absorption and rectification of the kinetic energy of the droplet by the flexible substrate. Additionally, for low-viscosity liquids, if the droplet−substrate system oscillation period is faster than the inertia−capillary time of the droplet, the upward movement of the substrate is decoupled from the droplet oscillation, resulting in the observed contact time reduction. Furthermore, we tested the flexible materials under challenging icing conditions, and we presented supercooled droplet−substrate impact experiments on surfaces contaminated with ice nucleation promoters (AgI), where the time to partial droplet solidification was faster than the natural oscillation of a droplet, even at not extreme supercooling. This way, we demonstrated that flexible materials can even shed partially solidified droplets and overcome substrate adhesion using the above-mentioned mechanism. Therefore, we conclude that the design of flexible icephobic materials should be based on their ability to store the droplet kinetic energy and release it at a later time, facilitated by the low areal density and moderate stiffness, as our theoretical modeling reveals.

ASSOCIATED CONTENT

Supporting Information

The Supporting Information is available free of charge on the ACS Publications website at DOI: 10.1021/acs.langmuir.7b01412.

Additional data and supporting figures on the surface impalement resistance characterization and droplet maximum spreading, details on the calculation of the rate of critical ice embryo formation, supporting figures on the surface characterization, experimental setup, and impacts of honey droplets, and detailed description of the movie files (DOCX)

Contact time reduction on flexible surfaces illustrated with a side-by-side comparison of droplets of different viscosities and droplets of different diameters impacting flexible superhydrophobic substrates (AVI)

Critical We for contact time reduction for water droplets illustrated with a side-by-side comparison of water droplets impacting superhydrophobic substrates above and below We_c (AVI)

Critical We for contact time reduction for glycerol droplets illustrated with a side-by-side comparison of glycerol droplets impacting flexible superhydrophobic substrates above and below We_c (AVI)

Honey droplets impacting flexible superhydrophobic substrates, with the honey droplets sticking on the surface or rebounding, depending on the We of the impact (AVI)

Measurement of the solidification rate ($1/t_f$) of supercooled droplets illustrated with a droplet impacting a flexible surface contaminated with AgI particles (AVI)

Repellency of solidified droplets illustrated with a side-by-side comparison between rigid and flexible substrates for three cases with respect to the solidification ($1/t_f$) and rebound ($1/t_c$) rates (AVI)

AUTHOR INFORMATION

Corresponding Authors

*E-mail: thomschu@ethz.ch.

*E-mail: dimos.poulikakos@ethz.ch.

ORCID

Thomas Vasileiou: 0000-0002-9342-7948

Thomas M. Schutzius: 0000-0003-3309-3568

Dimos Poulikakos: 0000-0001-5733-6478

DOI: 10.1021/acs.langmuir.7b01412
Langmuir 2017, 33, 6708−6718

Author Contributions

All authors conceived and designed the research. T.V. conducted the experiments and analyzed the data. All authors wrote the manuscript.

Notes

The authors declare no competing financial interest.

■ ACKNOWLEDGMENTS

Partial support of the Swiss National Science Foundation under Grant No. 162565 and the European Research Council under Advanced Grant No. 669908 (INTICE) is acknowledged.

■ REFERENCES

(1) Cebeci, T.; Kafyeke, F. Aircraft icing. *Annu. Rev. Fluid Mech.* **2003**, *35*, 11−21.
(2) Cao, Y. H.; Wu, Z. L.; Su, Y.; Xu, Z. D. Aircraft flight characteristics in icing conditions. *Prog. Aerosp Sci.* **2015**, *74*, 62−80.
(3) Lamraoui, F.; Fortin, G.; Benoit, R.; Perron, J.; Masson, C. Atmospheric icing impact on wind turbine production. *Cold Reg. Sci. Technol.* **2014**, *100*, 36−49.
(4) Davis, N. N.; Pinson, P.; Hahmann, A. N.; Clausen, N. E.; Zagar, M. Identifying and characterizing the impact of turbine icing on wind farm power generation. *Wind Energy* **2016**, *19* (8), 1503−1518.
(5) Huneault, M.; Langheit, C.; St-Arnaud, R.; Benny, J.; Audet, J.; Richard, J. C. A dynamic programming methodology to develop de-icing strategies during ice storms by channeling load currents in transmission networks. *IEEE Trans. Power Delivery* **2005**, *20* (2), 1604−1610.
(6) Fu, P.; Farzaneh, M.; Bouchard, G. Two-dimensional modelling of the ice accretion process on transmission line wires and conductors. *Cold Reg. Sci. Technol.* **2006**, *46* (2), 132−146.
(7) Pobanz, B. M.; Marwitz, J. D.; Politovich, M. K. Conditions Associated with Large-Drop Regions. *J. Appl. Meteorol* **1994**, *33* (11), 1366−1372.
(8) Zerr, R. J. Freezing rain: An observational and theoretical study. *J. Appl. Meteorol* **1997**, *36* (12), 1647−1661.
(9) Houston, T. G.; Changnon, S. A. Freezing rain events: a major weather hazard in the conterminous US. *Nat. Hazards* **2007**, *40* (2), 485−494.
(10) Jung, S.; Tiwari, M. K.; Doan, N. V.; Poulikakos, D. Mechanism of supercooled droplet freezing on surfaces. *Nat. Commun.* **2012**, *3*, 615.
(11) Dehaoui, A.; Issenmann, B.; Caupin, F. Viscosity of deeply supercooled water and its coupling to molecular diffusion. *Proc. Natl. Acad. Sci. U. S. A.* **2015**, *112* (39), 12020−12025.
(12) Maitra, T.; Antonini, C.; Tiwari, M. K.; Mularczyk, A.; Imeri, Z.; Schoch, P.; Poulikakos, D. Supercooled Water Drops Impacting Superhydrophobic Textures. *Langmuir* **2014**, *30* (36), 10855−10861.
(13) Carpenter, K.; Bahadur, V. Saltwater icephobicity: Influence of surface chemistry on saltwater icing. *Sci. Rep.* **2015**, *5*, 17563.
(14) Khedir, K. R.; Kannarpady, G. K.; Ishihara, H.; Woo, J.; Asar, M. P.; Ryerson, C.; Biris, A. S. Temperature-dependent bouncing of super-cooled water on Teflon-coated superhydrophobic tungsten nanorods. *Appl. Surf. Sci.* **2013**, *279*, 76−84.
(15) Boinovich, L. B.; Emelyanenko, A. M. Anti-icing potential of superhydrophobic coatings. *Mendeleev Commun.* **2013**, *23* (1), 3−10.
(16) Hao, C. L.; Liu, Y. H.; Chen, X. M.; Li, J.; Zhang, M.; Zhao, Y. H.; Wang, Z. K. Bioinspired Interfacial Materials with Enhanced Drop Mobility: From Fundamentals to Multifunctional Applications. *Small* **2016**, *12* (14), 1825−1839.
(17) Schutzius, T. M.; Jung, S.; Maitra, T.; Eberle, P.; Antonini, C.; Stamatopoulos, C.; Poulikakos, D. Physics of Icing and Rational Design of Surfaces with Extraordinary Icephobicity. *Langmuir* **2015**, *31* (17), 4807−4821.
(18) Mishchenko, L.; Hatton, B.; Bahadur, V.; Taylor, J. A.; Krupenkin, T.; Aizenberg, J. Design of Ice-free Nanostructured Surfaces Based on Repulsion of Impacting Water Droplets. *ACS Nano* **2010**, *4* (12), 7699−7707.
(19) Boreyko, J. B.; Collier, C. P. Delayed Frost Growth on Jumping-Drop Superhydrophobic Surfaces. *ACS Nano* **2013**, *7* (2), 1618−1627.
(20) Maitra, T.; Tiwari, M. K.; Antonini, C.; Schoch, P.; Jung, S.; Eberle, P.; Poulikakos, D. On the Nanoengineering of Superhydrophobic and Impalement Resistant Surface Textures below the Freezing Temperature. *Nano Lett.* **2014**, *14* (1), 172−182.
(21) Tourkine, P.; Le Merrer, M.; Quéré, D. Delayed Freezing on Water Repellent Materials. *Langmuir* **2009**, *25* (13), 7214−7216.
(22) Guo, P.; Zheng, Y. M.; Wen, M. X.; Song, C.; Lin, Y. C.; Jiang, L. Icephobic/Anti-Icing Properties of Micro/Nanostructured Surfaces. *Adv. Mater.* **2012**, *24* (19), 2642−2648.
(23) Eberle, P.; Tiwari, M. K.; Maitra, T.; Poulikakos, D. Rational nanostructuring of surfaces for extraordinary icephobicity. *Nanoscale* **2014**, *6* (9), 4874−4881.
(24) Jung, S.; Dorrestijn, M.; Raps, D.; Das, A.; Megaridis, C. M.; Poulikakos, D. Are Superhydrophobic Surfaces Best for Icephobicity? *Langmuir* **2011**, *27* (6), 3059−3066.
(25) Meuler, A. J.; Smith, J. D.; Varanasi, K. K.; Mabry, J. M.; McKinley, G. H.; Cohen, R. E. Relationships between Water Wettability and Ice Adhesion. *ACS Appl. Mater. Interfaces* **2010**, *2* (11), 3100−3110.
(26) Davis, A.; Yeong, Y. H.; Steele, A.; Bayer, I. S.; Loth, E. Superhydrophobic nanocomposite surface topography and ice adhesion. *ACS Appl. Mater. Interfaces* **2014**, *6* (12), 9272−9.
(27) Boreyko, J. B.; Srijanto, B. R.; Nguyen, T. D.; Vega, C.; Fuentes-Cabrera, M.; Collier, C. P. Dynamic Defrosting on Nanostructured Superhydrophobic Surfaces. *Langmuir* **2013**, *29* (30), 9516−9524.
(28) Bartolo, D.; Bouamrirene, F.; Verneuil, E.; Buguin, A.; Silberzan, P.; Moulinet, S. Bouncing or sticky droplets: Impalement transitions on superhydrophobic micropatterned surfaces. *Europhys. Lett.* **2006**, *74* (2), 299−305.
(29) Boreyko, J. B.; Baker, C. H.; Poley, C. R.; Chen, C. H. Wetting and Dewetting Transitions on Hierarchical Superhydrophobic Surfaces. *Langmuir* **2011**, *27* (12), 7502−7509.
(30) Deng, X.; Schellenberger, F.; Papadopoulos, P.; Vollmer, D.; Butt, H. J. Liquid Drops Impacting Superamphiphobic Coatings. *Langmuir* **2013**, *29* (25), 7847−7856.
(31) Nguyen, T. P. N.; Brunet, P.; Coffinier, Y.; Boukherroub, R. Quantitative Testing of Robustness on Superomniphobic Surfaces by Drop Impact. *Langmuir* **2010**, *26* (23), 18369−18373.
(32) Antonini, C.; Jung, S.; Wetzel, A.; Heer, E.; Schoch, P.; Moqaddam, A. M.; Chikatamarla, S. S.; Karlin, I.; Marengo, M.; Poulikakos, D. Contactless prompt tumbling rebound of drops from a sublimating slope. *Phys. Rev. Fluids* **2016**, *1* (1), 013903.
(33) Cao, L. L.; Jones, A. K.; Sikka, V. K.; Wu, J. Z.; Gao, D. Anti-Icing Superhydrophobic Coatings. *Langmuir* **2009**, *25* (21), 12444−12448.
(34) Vasileiou, T.; Gerber, J.; Prautzsch, J.; Schutzius, T. M.; Poulikakos, D. Superhydrophobicity enhancement through substrate flexibility. *Proc. Natl. Acad. Sci. U. S. A.* **2016**, *113* (47), 13307−13312.
(35) Weisensee, P. B.; Tian, J. J.; Miljkovic, N.; King, W. P. Water droplet impact on elastic superhydrophobic surfaces. *Sci. Rep.* **2016**, *6*, 30328.
(36) Liu, Y. H.; Moevius, L.; Xu, X. P.; Qian, T. Z.; Yeomans, J. M.; Wang, Z. K. Pancake bouncing on superhydrophobic surfaces. *Nat. Phys.* **2014**, *10* (7), 515−519.
(37) Moevius, L.; Liu, Y. H.; Wang, Z. K.; Yeomans, J. M. Pancake Bouncing: Simulations and Theory and Experimental Verification. *Langmuir* **2014**, *30* (43), 13021−13032.
(38) Schutzius, T. M.; Bayer, I. S.; Tiwari, M. K.; Megaridis, C. M. Novel Fluoropolymer Blends for the Fabrication of Sprayable Multifunctional Superhydrophobic Nanostructured Composites. *Ind. Eng. Chem. Res.* **2011**, *50* (19), 11117−11123.
(39) Schutzius, T. M.; Graeber, G.; Elsharkawy, M.; Oreluk, J.; Megaridis, C. M. Morphing and vectoring impacting droplets by means of wettability-engineered surfaces. *Sci. Rep.* **2014**, *4*, 7029.

DOI: 10.1021/acs.langmuir.7b01412
Langmuir 2017, 33, 6708−6718

(40) Cheng, N. S. Formula for the viscosity of a glycerol-water mixture. *Ind. Eng. Chem. Res.* **2008**, *47* (9), 3285−3288.
(41) Takamura, K.; Fischer, H.; Morrow, N. R. Physical properties of aqueous glycerol solutions. *J. Pet. Sci. Eng.* **2012**, *98*−*99*, 50−60.
(42) Milionis, A.; Fragouli, D.; Martiradonna, L.; Anyfantis, G. C.; Cozzoli, P. D.; Bayer, I. S.; Athanassiou, A. Spatially Controlled Surface Energy Traps on Superhydrophobic Surfaces. *ACS Appl. Mater. Interfaces* **2014**, *6* (2), 1036−1043.
(43) Burden, R. L.; Faires, J. D. *Numerical Analysis*, 9th ed.; Brooks/Cole, Cengage Learning: Boston, MA, 2011; p xiv, 872 pp.
(44) Holten, V.; Sengers, J. V.; Anisimov, M. A. Equation of State for Supercooled Water at Pressures up to 400 MPa. *J. Phys. Chem. Ref. Data* **2014**, *43* (4), 043101.
(45) Hruby, J.; Vins, V.; Mares, R.; Hykl, J.; Kalova, J. Surface Tension of Supercooled Water: No Inflection Point down to-25 degrees C. *J. Phys. Chem. Lett.* **2014**, *5* (3), 425−428.
(46) Marcolli, C.; Nagare, B.; Welti, A.; Lohmann, U. Ice nucleation efficiency of AgI: review and new insights. *Atmos. Chem. Phys.* **2016**, *16* (14), 8915−8937.
(47) Bird, J. C.; Dhiman, R.; Kwon, H. M.; Varanasi, K. K. Reducing the contact time of a bouncing drop. *Nature* **2013**, *503* (7476), 385−388.
(48) Lamb, H. On the oscillations of a viscous spheroid. *Proc. London Math. Soc.* **1881**, *s1-13* (1), 51−70.
(49) Schellart, W. P. Rheology and density of glucose syrup and honey: Determining their suitability for usage in analogue and fluid dynamic models of geological processes. *J. Struct. Geol.* **2011**, *33* (6), 1079−1088.
(50) Soto, D.; De Lariviere, A. B.; Boutillon, X.; Clanet, C.; Quéré, D. The force of impacting rain. *Soft Matter* **2014**, *10* (27), 4929−4934.
(51) Gart, S.; Mates, J. E.; Megaridis, C. M.; Jung, S. Droplet Impacting a Cantilever: A Leaf-Raindrop System. *Phys. Rev. Appl.* **2015**, *3* (4), 044019.
(52) Bartolo, D.; Josserand, C.; Bonn, D. Retraction dynamics of aqueous drops upon impact on non-wetting surfaces. *J. Fluid Mech.* **2005**, *545*, 329−338.
(53) Clanet, C.; Beguin, C.; Richard, D.; Quéré, D. Maximal deformation of an impacting drop. *J. Fluid Mech.* **1999**, *517*, 199−208.
(54) Butt, H. J.; Gao, N.; Papadopoulos, P.; Steffen, W.; Kappl, M.; Berger, R. Energy Dissipation of Moving Drops on Superhydrophobic and Superoleophobic Surfaces. *Langmuir* **2017**, *33* (1), 107−116.
(55) Olin, P.; Lindstrom, S. B.; Pettersson, T.; Wagberg, L. Water Drop Friction on Superhydrophobic Surfaces. *Langmuir* **2013**, *29* (29), 9079−9089.
(56) Bartolo, D.; Boudaoud, A.; Narcy, G.; Bonn, D. Dynamics of non-Newtonian droplets. *Phys. Rev. Lett.* **2007**, *99* (17), 174502.
(57) Jung, S.; Tiwari, M. K.; Poulikakos, D. Frost halos from supercooled water droplets. *Proc. Natl. Acad. Sci. U. S. A.* **2012**, *109* (40), 16073−16078.
(58) Ickes, L.; Welti, A.; Hoose, C.; Lohmann, U. Classical nucleation theory of homogeneous freezing of water: thermodynamic and kinetic parameters. *Phys. Chem. Chem. Phys.* **2015**, *17* (8), 5514−5537.
(59) Barthlott, W.; Neinhuis, C. Purity of the sacred lotus, or escape from contamination in biological surfaces. *Planta* **1997**, *202* (1), 1−8.

DOI: 10.1021/acs.langmuir.7b01412
Langmuir 2017, 33, 6708−6718